Langmuir

Article

pubs.acs.org/Langmuir

Microfluidic Production of Spherical and Nonspherical Fat Particles by Thermal Quenching of Crystallizable Oils

Jihye Kim and Siva A. Vanapalli*

Department of Chemical Engineering, Texas Tech University, Lubbock, Texas 79409, United States

Supporting Information

ABSTRACT: We report the microfluidic production of spherical and nonspherical fat particles from crystallizable oils. The method is based on microfluidic generation of oil droplets at a cross-junction followed by thermal solidification downstream in a microcapillary. We vary the drop production conditions and the device temperature and demonstrate that the size, shape, and crystallinity can be controlled. By measuring thermal gradients in the microcapillary, we show that crystalline fat particles are best produced when the device temperature is below the onset temperature of bulk fat crystallization. To produce monodisperse nonspherical fat particles, we find that the carrier fluid flow rate needs to be sufficiently high to provide strong hydrodynamic forces to transport the confined rod-like particles. We identify the scaling relationship between geometric confinement and particle elasticity necessary to maintain the nonspherical shape. Thus, our study provides guidelines for the production of spherical and nonspherical fat particles that can be potentially used for controlling microstructure, rheology, and drug encapsulation in foods, cosmetics, and pharmaceutical creams that employ crystallizable oils.

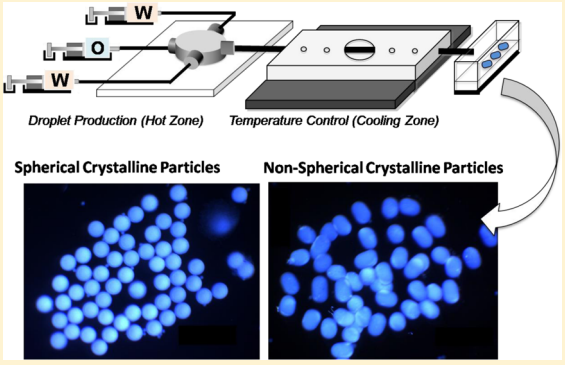

I. INTRODUCTION

There has been growing interest in controlling the size, shape, and composition of microparticles for applications in foods, personal care products, biotechnology, advanced materials, and pharmaceuticals. Microparticles with tailored properties have the potential to provide a variety of new capabilities including controlling the rheology of complex fluids[1] and kinetics of drug release.[2] Current techniques available to produce these so-called "designer particles" have been highlighted in recent reviews.[3−6] In this study, we use microfluidics to engineer spherical and nonspherical fat particles from crystallizable oils.

The use of crystallizable oils to generate microparticles of controlled size and shape has significant practical applications. Emulsions made from crystallizable fats are an essential component of food products such as ice cream and butter.[7−9] In this case, crystallizable fats crucially control the mouthfeel and flavor release of foods. Likewise, pharmaceutical and cosmetic products such as ointments and topical creams rely on crystallizable oils to facilitate drug encapsulation and soft texture.[10,11] The manufacture of these products often involves hot emulsification of crystallizable oils (and other additives) followed by thermal quenching and shear. Such bulk processing methods do not provide adequate control over the properties of individual fat particles. Since particle size, composition, and shape regulate the microstructure, rheology, and drug release kinetics, development of methods to exquisitely control the properties of fat particles will lead to products with improved functionality. For example, fabrication of fat particles of nonspherical shape can generate larger viscosity than their spherical counterparts at the same volume fraction,[1] enabling the production of dispersions with low fat content without compromising the viscosity or texture of the product.

Recent developments in microfluidics open new possibilities for designing dispersions with fine control of individual particle properties.[12−15] In particular, drop-based microfluidics has become a very efficient and simple means to produce monodisperse single droplets[16−18] as well as compound drops.[12,19] In addition to emulsions containing spherical droplets, droplet-based microfluidics has also been used to fabricate nonspherical particles using drops as precursors.[3] Geometric confinement of droplets in microfluidic channels followed by UV-induced polymerization has been used to produce nonspherical microparticles.[20−23] Doughnut-shaped toroidal structures were also fabricated using asymmetric polymer solidification.[24] Particle shape was also controlled by elasticity-induced arrested coalescence of two or more droplets.[25,26] In addition, nonspherical particles have been fabricated by cross-linking biopolymers (e.g., alginate, chitosan) within microfluidic droplets.[27−30]

In this study, motivated by practical applications that employ crystallizable oils we explore the use of drop-based microfluidics and thermal quenching to control the crystallinity, size, and shape of fat particles. Unlike chemical cross-linking strategies employed in microfluidic methods discussed above, we harness

Received: April 9, 2013
Revised: August 4, 2013
Published: September 3, 2013

   dx.doi.org/10.1021/la401338m | *Langmuir* 2013, 29, 12307−12316

thermal quenching as a new physical method to fabricate fat particles of spherical and nonspherical shape. We note that microfluidic drops in combination with thermal quenching has been used to investigate the thermodynamics of nucleation in simple liquids.[31−36] The focus of this work is on fabricating novel particles from a new class of soft materials, i.e., crystallizable oils. This distinction in focus requires addressing new scientific questions. How are channel temperatures (or thermal gradients) needed to solidify particles related to the crystallization behavior of the oils that contain a mixture of fatty acids? For the production of nonspherical particles, what level of particle elasticity or deformability is needed to hydrodynamically transport the particles without jamming the channels? We address these questions by investigating the relationship between fluid flow, particle confinement, and heat transfer. On the basis of this investigation, we provide design rules for the production of spherical and nonspherical fat particles from crystallizable oils.

II. MATERIALS AND METHODS

II.A. Materials and Preparation. In our study, we used palm oil as the crystallizable fat due its relevance in food and pharmaceutical industry.[37] Palm oil (Sans trans, Loders Croklaan, Channahon, IL) and 2 wt % poly(ethylene glycol) sorbitan monolaurate (Tween 20, Sigma-Aldrich, St. Louis, MO) solution were used as the dispersed and continuous phases, respectively. To prepare solution for experiment, palm oil was melted, filtered (Minisart pore size of 5 μm, Sartorius stedim biotech, France), and placed in a vacuum desiccator (Bel-art products) to remove air bubbles. The aqueous phase was also similarly filtered and degassed prior to experiment. The interfacial tension (γ) at 70 °C between liquid palm oil and 2 wt % Tween 20 was measured to be 5.06 ± 0.33 mN/m using the pendant drop method.[38,39]

II.B. Thermal and Rheological Characterization of Palm Oil. The crystallization and mechanical properties of palm oil are expected to regulate the crystallinity and shape of the fat particles produced; we therefore measured the melting temperature, onset of crystallization, and rheological properties of bulk palm oil. This physical characterization also helped in designing the range of operating conditions for the microfluidic setup and in interpreting the results from the microfluidic experiments.

Palm oil is a mixture of different types of fatty acids (palmitic, stearic, myristic, oleic, and linoleic acids) and thus has a broad melting point. To characterize the crystallization and melting properties of palm oil, the solid fat content (SFC) of palm oil was measured at different temperatures using nuclear magnetic resonance (Brukerminispec pulsed-field NMR, Bruker Optics, Billerica, MA). Samples were prepared for SFC analysis by pouring molten palm oil into NMR tubes and refrigerating for 3.5 days. Subsequently, samples were held in a water bath at the specified temperature for an hour before taking a measurement. The measurement was repeated three times. Our results in Figure 2a show that the melting point of this fat as characterized by NMR is T_m = 35 °C.

The onset of crystallization as a function of cooling rates was characterized using differential scanning calorimetry (DSC822e, Mettler Toledo, Columbus, OH). Approximately 5 mg of palm oil sample was loaded into a sealed aluminum pan and melted at 70 °C for 2 min to erase crystal memory and subsequently cooled to −40 °C at different cooling rates (1−20 °C/min). Heat flux was measured relative to an empty pan. Figure 2b shows a representative thermogram obtained from the differential scanning calorimeter (DSC). The plot shows two distinct exothermic peaks, with the onset of crystallization, T_{onset} = 20.1 °C. We found T_{onset} varied from 20.1 to 16.5 °C when the cooling rate was varied from 1 to 20 °C/min. The total enthalpy associated with crystallization and polymorphic transformations was determined from the total area under the heat flux curve and was found to be 47.8 J/g regardless of the cooling rate.

The linear viscoelastic properties of the palm fat were determined as a function of temperature by small-amplitude oscillatory shear tests in a rheometer (AR2000, TA Instruments, New castle, DE). The measurements were conducted in a plate−plate geometry with a gap of 0.5 mm at an applied strain of 0.1%, oscillation frequency of 1 Hz, and prescribed cooling rate (1, 3, and 5 °C/min). The runs were repeated three times. Figure 2c shows that the elastic modulus (G') as a function of temperature at a cooling rate of 3 °C/min. The loss moduli values (G'') were about 1 order of magnitude lower than G', indicating that the fat sample upon cooling displayed solid-like behavior. As expected, G' increased as the temperature decreased due to increased solid fat content.

II.C. Assembly of Microfluidic Device. As shown in Figure 1, our setup includes both a drop-production unit and spatially regulated thermal control to heat and cool the fluids. This setup resembles that of Stan et al.,[32] who studied the nucleation of ice crystals in microfluidic water drops. These authors used microfabrication techniques to fabricate both the channels and thermal resistors (for-on-chip cooling and heating). In contrast, as discussed below, we used off-the-shelf components to both produce the drops and subject the fluids to thermal treatment.

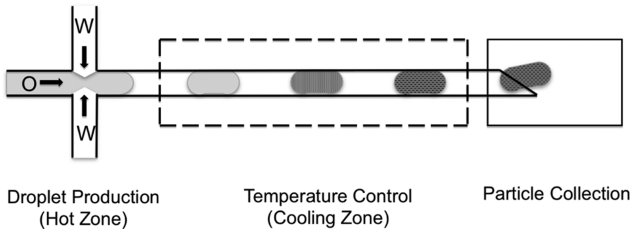

Figure 1. Basic principle of microfluidic production of fat particles from crystallizable oils. Liquid microfluidic droplets produced at the cross-junction can be subsequently cooled to induce crystallization. Depending on the degree of drop confinement, either spherical or nonspherical fat particles can be produced. The illustration shows solidified particles exiting from the capillary and retaining their nonspherical shape.

To produce emulsions containing oil droplets in an aqueous continuous phase, the device walls need to be hydrophilic to ensure good wettability of the water phase.[17] We assembled a fluidic device with hydrophilic wettability using commercially obtained parts and fittings. The drop generator is a stainless steel cross (Valco, ZX1M, tubing o.d. 1/16 in.) with an inner circular bore of diameter 500 μm (see Figure 3a). A silica-coated microcapillary (Supelco 25709) of inner diameter D = 530 μm and length L = 7.8 cm was connected downstream of the drop generator to confine the droplets and induce lipid crystallization. To image the moving droplets inside the microcapillary, the polyimide coating on the outer surface was removed (by gentle burning of the coating and scratching with a razor) to make the middle and tail portions of the capillary transparent. The end of the microcapillary was diagonally cut to prevent jamming of high aspect ratio rod-shaped particles at the time of exit. To establish a smooth connection between the head of the microcapillary and the cross-fitting, the front end was polished with a sandpaper (3M, 220-320-400, P400). The coupling between the capillary and the cross-fitting was made using Tygon tubings (Cole Parmer, i.d. 0.022 in., o.d. 0.042 in.; MicroMix, i.d. 0.04 in., o.d. 0.07 in.) and fortifying them with cross-linked polydimethylsiloxane (PDMS) (see Supporting Information Figure ESI.1).

II.D. Temperature Control Setup. To produce fat particles, preheated liquid oil droplets generated by the cross-flow geometry were transported through a cooling zone as shown in Figure 3. To prevent premature crystallization of palm oil during the droplet production process, the cross-junction device as well as the tubing containing the aqueous phase was placed on a hot plate (Fisher Scientific, 11-100-49H) set at 70 °C. Preheating of the dispersed phase was achieved by loading liquid palm oil into a syringe (BD vacutainer,

dx.doi.org/10.1021/la401338m | Langmuir 2013, 29, 12307−12316

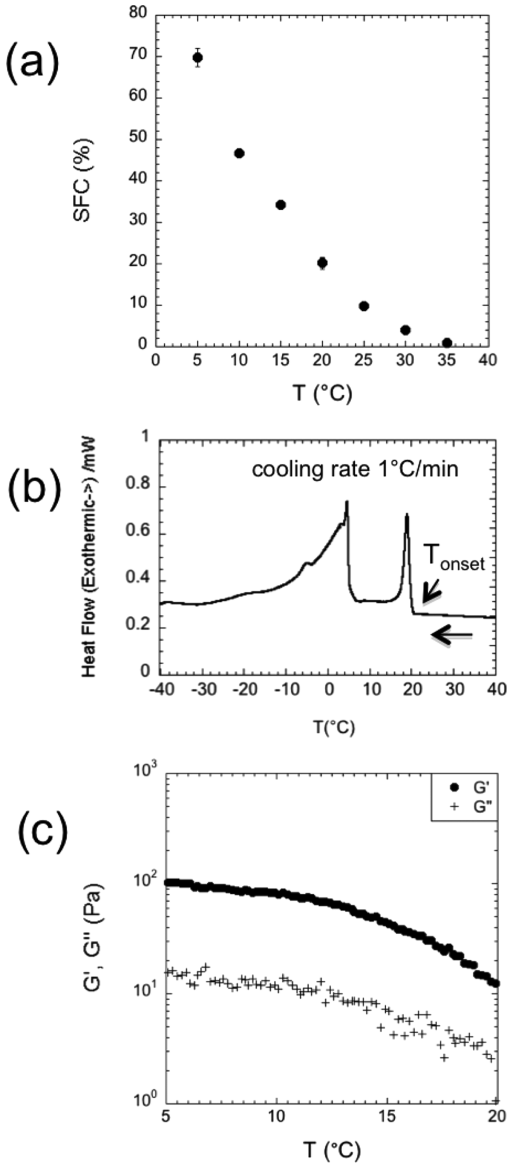

Figure 2. (a) Solid fat content (SFC) of palm oil measured using NMR, (b) heat associated with crystallization of palm oil measured using DSC, and (c) storage (G') and loss (G'') modulus of palm oil measured using a rheometer at cooling rate of 3 °C/min.

Labware Medical) and wrapping the syringe using thermal rope. Another thermal rope was placed on the capillary tubing at the gap between the stainless steel cross fitting and the cooling zone (where it was exposed to the air) to ensure the droplets were liquid before entering the cooling zone. The temperature of thermal ropes was set to 70 °C by temperature controllers (Omega, Stamford, CT, CN7800).

To cool the preheated liquid oil droplets in the capillary tubing, a cooling chamber was designed that controlled the temperature of the capillary. The cooling chamber consisted of a custom-made aluminum block (7.8 cm × 5.2 cm × 3 cm) that was in contact with a Pelteir-based thermal stage (see Figure 3b). The custom-made metal block had a longitudinal bore (diameter of 3 mm) to hold the capillary, four transverse bores (diameter of 3 mm) for the insertion of thermocouples and central circular window (diameter of 1.5 cm) for optical access (see Figure 3c). The thermal stage (TSA02I, Instec, Boulder, CO) as shown in Figure 3b was used to control the temperature of the metal block from 5 to 50 °C, using a programmable controller (Instec, STC200), software (Instec, wintemp), and a refrigerated water bath as heat sink.

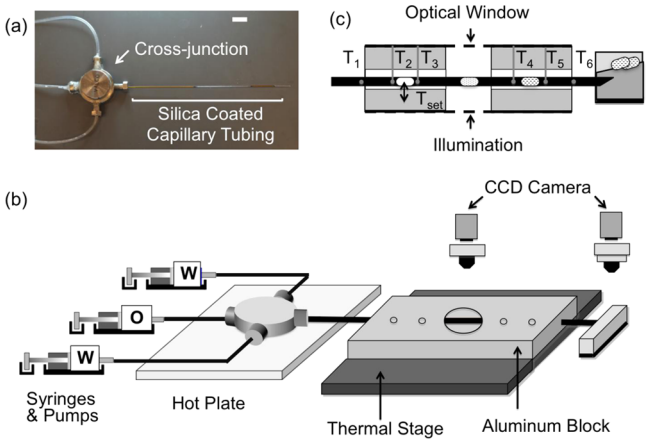

Figure 3. (a) An image of the assembled cross-junction device for producing fat droplets dispersed in an aqueous phase. Scale bar is 1 cm. (b) Schematic of the experiment setup showing fluid delivery by the pumps into the cross-junction device, preheating of the fluids by a hot plate, and subsequent cooling and visualization of the fat droplets (c) Schematic of the cross-sectional view of the microcapillary that is housed in the cooling chamber. Cooling is achieved by a combination of the thermal stage and the aluminum block. The thermal stage is used to prescribe the temperature T_{set}, and thermocouples are used to measure the local temperature T_i (i = 1−6) along the microcapillary. Optical access is provided for imaging.

Since crystallization of fat droplets depends critically on thermal history, we recorded the temperature profile along the microcapillary by placing fine wire thermocouples (part no. 5TC-TT-K-40-36, Omega, Stamford, CT) at six different locations (T_1 to T_6) along the capillary as shown in Figure 3c. The temperatures were recorded with an error of ±1 °C. Four thermcouples recorded the temperatures of the section of the capillary housed inside the custom-made metal block, and the other two were located at the inlet and outlet of the metal block. The six temperatures were simultaneously measured every minute using a combination of data aquisition board (Omega, TC08) and software (Logging software 5.21.6, Omega).

II.E. Flow Control. To produce droplets, a syringe filled with palm oil was connected to one of the inlets of the cross and two syringes charged with 2 wt % Tween20 solution were connected to each of the side inlets (see Figure 3b). All the inlet ports connected with tubing were sealed with cross-linked PDMS to remove any source of air entering into the cross-junction device. The fluids in syringes were discharged with a controlled volumetric flow rate by using syringe pumps (KD Scientific, Holliston, MA). Flow rate of the inner phase, palm oil, was fixed at Q_o = 0.1 mL/h for all experiments, and the flow rate of the outer aqueous phase was varied from Q_w = 0.5−20 mL/h. Note that Q_w refers to the sum of the flow rates from the two side channels. Under these flow conditions, the droplet production rate was found to be 12−36 droplets/min.

II.F. Microscopy and Image Analysis. The moving droplets potentially undergoing phase transition in the microcapillary were observed at two locations (i) at the window in the middle of the cooling zone and (ii) at the exit of the capillary. At the circular window in the custom-made metal block, droplets were visualized using a stereo microscope (Stemi 2000-C, Zeiss, Thornwood, NY) in bright field and transmission mode and recorded using a CCD camera (STV-LRM, SVSi, Madison, AL). The movies taken were analyzed for droplet length and speed using Image J v.1.41o and Matlab R2010a. For each condition of temperature and flow rate, the number of droplets analyzed ranged from 11 to 42. To quantify the uniformity in droplet size, we define the polydispersity index, PDI = $100\sigma/L_d$, where σ is the standard deviation and L_d is the mean droplet length. We consider emulsions with PDI < 5% to be monodisperse.

To identify whether confined droplets would regain their spherical shape or retain their nonspherical shape (due to crystallization),

dx.doi.org/10.1021/la401338m | Langmuir 2013, 29, 12307−12316

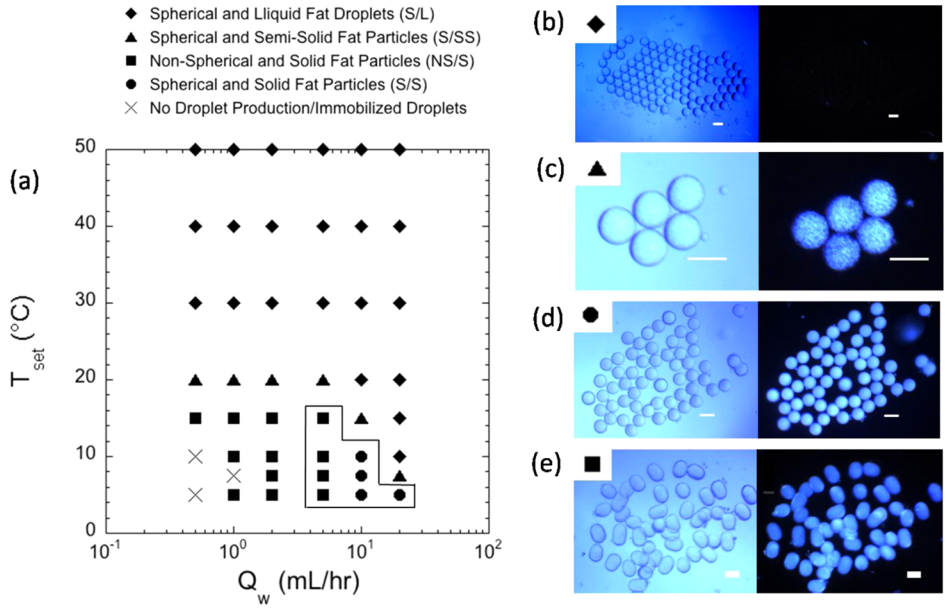

Figure 4. (a) Experimental state diagram showing the conditions at which different types of dispersed phase particles are produced. The zone highlighted by the black line indicates the conditions where solidified particles were produced with uniform droplet size (PDI < 10%); elsewhere, the solidified particle production was polydisperse. Optical micrographs under plane-polarized light (left) and cross-polarized light (right) are presented for: (b) Spherical and liquid fat droplets. T_{set}= 50 °C, Q_o = 0.1 mL/h, and Q_w = 2 mL/h. (c) Spherical and semisolid fat particles. T_{set} = 7.5 °C, Q_o = 0.1 mL/h, and Q_w= 20 mL/h. (d) Spherical and solid fat particles. T_{set} = 10 °C, Q_o = 0.1 mL/h, Q_w = 10 mL/h. (e) Nonspherical and solid fat particles. T_{set} = 10 °C, Q_o = 100 μL/h, and Q_w = 5 mL/h. Scale bar is 500 μm.

droplets were also observed as they exited the microcapillary using the same setup, with microscopy being done under reflection mode. To determine whether the droplets were liquid, partially crystallized, or fully solid, the produced droplets were collected at room temperature and observed immediately under another stereo microscope (Omano Microscope.com, Roanoke, VA) containing a polarizer (SZX2-AN, Olympus, Center Valley, PA) and analyzer (IX-AN T2, Olympus, Center Valley, PA).

II.G. Dimensionless Numbers. Three dimensionless numbers are relevant for this study. We define the Reynolds number, $Re = \rho VD/\mu$, where ρ (= 998 kg/m^3) and μ (= 1 mPa·s) are the density and viscosity of the continuous phase, respectively; V is the mean velocity of the continuous phase, and D is the inner diameter of the microcapillary. In this study, Re = 0.3−13.3, implying that inertia was non-negligible under certain flow conditions. The capillary number, $Ca = \mu V/\gamma$, was in the range of 1×10^{-3}−5×10^{-3}, indicating that capillary forces were dominant over viscous forces in the system. The Peclet number, $Pe = VD/\alpha$, was in the range 2.3−93.1, where $\alpha = 1.43 \times 10^{-7}$ m^2/s is thermal diffusivity of the continuous phase. Since Pe > 1, the rate of fluid convection is faster than the rate of heat diffusion in our system.

III. RESULT AND DISCUSSION

III.A. Production of Fat Particles of Different Morphology and Crystallinity. The ability to produce spherical and nonspherical fat particles depends on the droplet size relative to the capillary tube diameter. Moreover, the temperature needs to be low enough that the droplets undergo thermal solidification (see Figure 1). The droplet size is controlled by the flow rates of the dispersed and continuous phases, and in a cross-junction, drop size increases with decrease in continuous phase flow rate.[40] The temperature experienced by the droplets can be tuned by the temperature of the thermal stage (T_{set}) housing the cooling zone. In our experiments, we therefore varied the two control parameters: T_{set} = 5−50 °C and the flow rate of the aqueous phase, Q_w = 0.5−20 mL/h. The oil flow rate was kept constant at Q_o = 0.1 mL/h. By collecting all the observations in our experiments, we find four different types of fat particles based on their shape and degree of crystallinity as shown in Figure 4: (i) spherical and liquid (S/L) fat droplets, (ii) spherical and semisolid (S/SS) fat particles, (iii) spherical and solid (S/S) fat particles, and (iv) nonspherical and solid (N/S) fat particles. The state diagram at which we obtain these different fat particles is shown in Figure 4a, and representative images of these particles are shown in Figure 4b−e.

For $T_{set} \geq$ 30 °C, under all explored aqueous flow rates, we found that the fat droplets were spherical and liquid. The S/L fat droplets were not visible under cross-polarized microscopy, indicating the lack of internal fat crystals. Moreover, despite being confined in the cooling zone, they retained a spherical shape in the collection zone without coalescence with other droplets, confirming the absence of a strong elastic fat crystal network (see Supporting Information movie ESI.2a). These findings suggest that for $T_{set} \geq$ 30 °C, irrespective of the explored flow rate, crystal nucleation and growth do not occur in the droplets. Interestingly, S/L fat droplets were also found at lower temperatures, only when the carrier fluid flow rates were high. For example, as shown in Figure 4a, S/L fat droplets were identified at T_{set} = 20 °C and Q_w = 10 mL/h as well as at $T_{set} \geq$ 10 °C and Q_w = 20 mL/h. These observations suggest that even though cooling temperature (T_{set}) is much lower than the bulk melting point, short residence times due to high continuous phase flow rates may lead to inefficient heat transfer from the cooling chamber to the fluid inside the microcapillary (see section III.B for further discussion), precluding nucleation and crystal growth in fat droplets.

When T_{set} was lowered to 20 °C, for Q_w < 10 mL/h, spherical and semisolid (S/SS) fat particles were produced in the collection zone. Birefringent fat crystals were visible under cross-polarizers; however, the internal texture was coarser and grainy, which was also evident by clear variations in the gray

dx.doi.org/10.1021/la401338m | Langmuir 2013, 29, 12307−12316

scale pixel intensity across the diameter of the drops (see Supporting Information Figure ESI.3a). Furthermore, S/SS fat particles retain spherical shape at the time of exit from microcapillary regardless of the degree of confinement in droplet size inside the capillary. Unlike the S/L fat droplets that did not coalesce upon exiting the capillary, we observed that the S/SS particles would often coalesce (see Supporting Information movie ESI.2b) and form larger spherical droplets. Since coalescence of semicrystalline emulsion droplets has been well documented through the mechanism of partial coalescence,[41,42] we suggest that these fat particles were actually semisolid rather than being fully solidified. The few other conditions where S/SS fat particles were found include T_{set} = 15 °C and Q_w = 10 mL/h and T_{set} = 7.5 °C and Q_w = 20 mL/h.

When the temperature of the cooling zone was further lowered to 15 °C and below, seemingly solid fat particles were found. Specifically, N/S fat particles were observed for $T_{set} \leq 15$ °C and $Q_w \leq 5$ mL/h, and S/S fat particles were obtained when $T_{set} \leq 10$ °C and Q_w = 10 mL/h. We note that although we refer to these particles as being solidified, they are not fully crystalline since the NMR and DSC data (cf. Figure 2a,b) show that even at 5 °C, the palm oil has only 70% SFC. However, both the N/S and S/S fat particles have higher SFC than S/SS particles because of the negligible variation in gray scale pixel intensity within the particles (as compared to that of S/SS fat particles) (see Supporting Information Figure ESI.3b). Moreover, we observed that neither the N/S particles nor the S/S particles coalesced downstream in the collection zone despite being in contact with each other, indicating that the SFC in these particles was much higher than that of S/SS particles, preventing partial coalescence (see Supporting Information movie ESI.2c). Previously, it has been shown that emulsion droplets, produced via bulk emulsification and with high SFC value, also do not coalesce with each other.[25]

At temperatures much lower than 10 °C, and under very low flow rates of the carrier fluid ($Q_w \leq 1$ mL/h), droplet production was considerably hampered because highly solidified fat particles jammed the microcapillary, preventing further production of droplets. The experimental conditions at which consistent and intermittent droplet production occurred are further discussed in section III.C.

III.B. Dynamics of Fat Crystallization in Moving Confined Droplets. The results of Figure 4 reveal that the formation of partially crystalline or solidified fat particles in the microcapillary depends on the interaction between fluid flow and thermal history experienced by the moving droplets. It is likely that varying the flow rates of the fluid modifies the rate of heat transfer resulting in different temperature gradients along the length of the microcapillary, influencing the types of fat particles produced. To gain insights into the optimal local temperatures needed to produce nonspherical fat particles, we measured the wall temperatures (T_{wall}) along the microcapillary at six different locations as shown in Figure 3c. We assume the wall temperature to be reflective of the local fluid temperature inside the microcapillary because in the slender microcapillary (length-to-diameter ratio = 1238), thermal gradients along the radial direction are negligible compared to those in the axial direction.

In Figure 5, we show thermal gradient profiles as a function of normalized downstream distance (x/L) for T_{set} = 15 °C. For all flow rates, the microcapillary wall temperature decreases with downstream distance, indicating that thermal energy is removed from the flowing hot emulsion by the surrounding

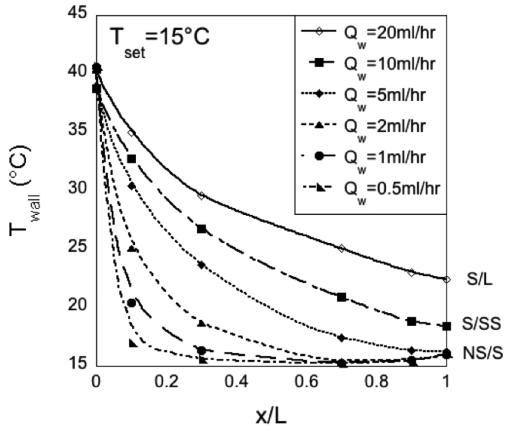

Figure 5. Temperature profile of the flow across the cooling zone from the inlet (x/L = 0) to the end of the cooling zone (x/L = 1) at T_{set} = 15 °C; the text indicates the final type of fat particles produced at the outlet.

medium. In particular, we find that higher continuous phase flow rates lead to shallow gradients in fluid temperature. In fact, for Q_w = 20 mL/h, or $Pe \approx 93$, the minimum fluid temperatures (T_6 near the capillary exit) do not even reach the set temperature and are about 10 °C higher than T_{set}. Thus, at higher continuous phase flow rates, convective flow dominates over heat conduction, making droplets experience higher temperatures than T_{set}. In contrast, at very low flow rates of the carrier fluid (e.g., Q_w = 0.5 mL/h, $Pe \approx 2$), the temperature gradients are much steeper, and the minimum fluid temperature reaches close to the set temperature. These observations indicate that low carrier fluid flow rates, or alternatively long residence times, allow effective heat transfer from the cooling metal block (housing the microcapillary) to the flowing confined droplets, enabling the drops to reach to the temperature close to T_{set}.

The resulting temperature gradients affect the types of particles produced at the outlet. As shown in Figure 5, we find that the shallow temperature gradients resulting from high flow rates (Q_w = 20 mL/h) produce only liquid fat droplets. However, the steeper thermal gradient profiles at low flow rates make the local wall temperatures to be much below the melting point of palm oil, enabling crystallization of fat droplets and producing S/SS and NS/S fat particles. Thus, both the temperature gradient and the flow rate (or residence time) play a crucial role in determining the crystallization of moving droplets.

To identify if there is a suitable combination of minimum temperature and residence time that produces crystalline droplets, we plot in Figure 6 the wall temperature just before the exit, T_6 (which is also the minimum wall temperature), and the corresponding residence time equivalent to a drop length (τ_d) for all the experimental conditions tested. Here we define $\tau_d = L_d/U$, where L_d and U are the mean droplet length and fluid velocity, respectively. Note that τ_d represents the duration that droplets were exposed to the lowest temperature and are not the total residence time experienced by the drops inside the whole length of the microcapillary. Interestingly, we find that when $T_6 \approx 20$ °C, almost all fat droplets are either in a partially crystalline (S/SS) or solidifed state (S/S and NS/S), implying that the critical value of $T_6 \approx 20$ °C represents the onset of nucleation in the microfluidic experiments. This observation also suggests that the residence time experienced by droplets

dx.doi.org/10.1021/la401338m | Langmuir 2013, 29, 12307−12316

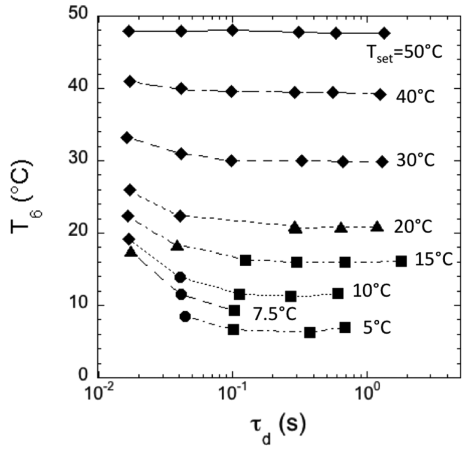

Figure 6. Relationship betweenthe lowest temperatureexperienced by fat droplets (T_6) and theresidence time (τ_d) in the cooling chamber. The labeled temperatures represent T_{set} values. The symbols represent the final product at the exit (◆) S/L, (▲) S/SS, (●) S/S, and (■) NS/S.

does not significantly impact nucleation in our experiments. The estimate of onset of crystallization obtained from the microfluidic expeirments is consistent with the onset of crystallization of 16.5−20.1 °C (for a cooling rate of 1−20 °C/min) measured with the DSC. Thus, it appears that regardless of the residence time, if the droplets experience a temperature close to the bulk fat crystallization temperature, nucleation is triggered. However, we find the residence time does impact the degree of crystallinity, since Figure 6 reveals that shorter residence times produce semisolid droplets (τ_d = 0.02 s, $T_6 \approx 17.6$ °C) and longer residence times yield solid particles (τ_d = 0.12 s, $T_6 \approx 16.2$ °C) at very similar wall temperatures.

III.C. Fidelity of Fat Particle Production. To determine the fidelity of the microfluidic production process, we assessed the uniformity in the size distribution of the particles produced. Figure 7a shows the polydispersity index (PDI) of the particles for all flow and temperature conditions explored. We find that the PDI for S/L droplets is very low (≤2%) for Q_w> 2 mL/h, indicating that the particles are essentially monodisperse. In contrast, for Q_w< 2 mL/h, the S/L fat droplets are marginally monodisperse (PDI ∼ 1−11%). The PDI values for S/SS fat particles as well as its dependence on carrier fluid flow rate are similar to that of the S/L fat droplets (PDI ∼ 1−13%). The S/S fat particles produced (only) at high flow rates are quite monodisperse (PDI ≤ 2%). The NS/S fat particles produced are polydisperse (see Figure 7c for a representative polydisperse emulsion) except at four experimental conditions, where they are monodisperse (see Figure 4e). Taken together, the data in Figure 7a indicate that significant polydispersity is observed for low carrier fluid flow rates ($Q_w \leq$ 2 mL/h) and stage temperatures ($T_{set} \leq$ 15 °C).

To understand the origins of significant polydispersity observed under certain flow and temperature conditions, we computed the coefficient of variation (CV) in droplet velocity, by analyzing the recorded movies. Figure 7b shows how the CV

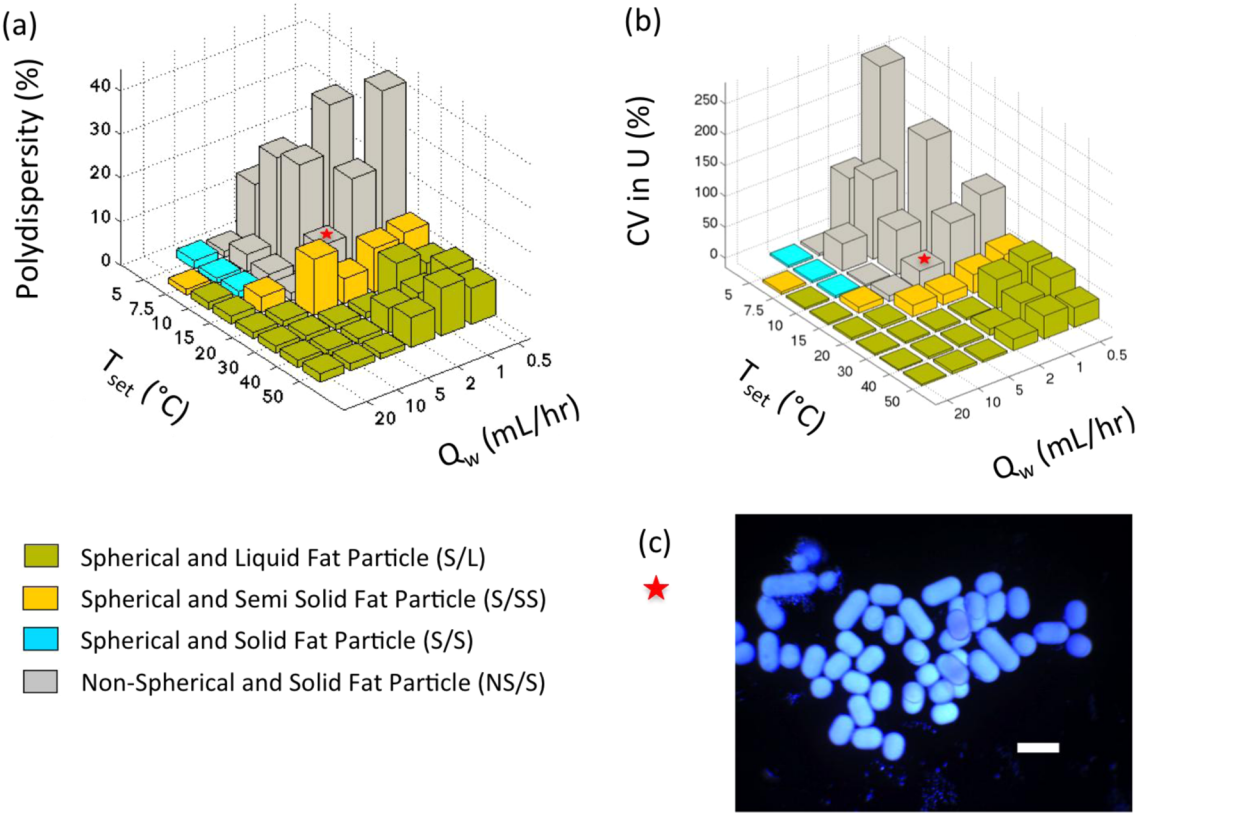

Figure 7. (a) Polydispersity in droplet size and (b) coefficient of variation in droplet speed as a function of the carrier fluid flow rate (Q_w) and the cooling zone temperature (T_{set}). (c) Polarized optical micrograph of polydisperse (PDI = 10%) nonspherical fat particles produced because of drop velocity fluctuations. The experimental conditions (T_{set} = 15 °C, Q_o = 100 μL/h, Q_w = 2 mL/h) corresponding to the production of this particle are highlighted with a red star in (a) and (b). Scale bar denotes 1 mm.

dx.doi.org/10.1021/la401338m | *Langmuir* 2013, 29, 12307−12316

of droplet velocity depends on Q_w and T_{set}. The trends in CV of droplet velocity are very similar to that of polydispersity variation, suggesting that fluctuations in droplet velocity are the main cause of polydispersity observed in our experiments.

We postulate two main mechanisms responsible for the fluctuations in droplet velocities. Both these mechanisms are linked to pressure fluctuations in the system. First, when droplets are being produced at the cross-junction in the so-called squeezing regime,[43] the protruding finger of the dispersed phase temporarily blocks the cylindrical orifice causing buildup of pressure upstream of the neck, just prior to breakup. Because of the cyclical production of drops, this pressure can fluctuate, causing variations in drop velocity. Such pressure fluctuations are most prominent at low carrier fluid flow rates, when the squeezing regime of drop breakup dominates. Second, the transport of confined particles through a cylindrical tube also causes excess pressure drop. The magnitude of this pressure drop depends on parameters such as level of particle confinement (i.e., ratio of particle to tube diameter), number of particles in the capillary, particle deformability, and carrier fluid flow rate.[44−46] Depending on the specific values of these parameters in the experiments, this pressure drop can severely restrict the flow of carrier fluid, causing buildup of pressure in the system. We note that although our fluids are driven by constant-flow-rate pumps and velocity fluctuations should be absent for a truly rigid fluidic system, we believe the combined effects of compliance in the tubing and pressure accumulation (due to the two mechanisms) cause fluctuations in drop speed in our experiments.

Our experimental observations of polydispersity dependence on the type of fat particles produced (cf. Figure 7) are qualitatively consistent with the mechanisms discussed above. The spherical solid (S/S) particles that were produced only at high aqueous flow rates are largely unconfined ($L_d/D \leq 1.06$), indicating that they do not offer significant pressure drop. Therefore, these particles are monodipserse and have low CV in drop velocity as shown in Figure 7. The spherical liquid droplets had also low polydispersity at higher flow rates ($Q_w >$ 2 mL/h) because of less confinement. But their polydispersity increased at low flow rates ($Q_w \leq 2$ mL/h) because of increased confinement (L_d/D = 1.46−1.7). Besides, the number of droplets present inside the microcapillary increases by 10 times at low flow rates compared to the high carrier fluid flow rates. The increase in the number of droplets in the microcapillary produces higher flow resistance downstream, contributing to inconsistent droplet generation at the orifice under low flow rates. Polydispersity gets further accentuated when drop deformability is reduced due to fat crystallization because Figure 7 shows that the nonspherical fat particles had generally higher polydispersity and CV in droplet velocity compared to spherical liquid drops, implying that their longer length and less deformability generates significant pressure fluctuations.

Thus, the fidelity in droplet production can be affected by the hydrodynamic resistance resulting from droplet confinement, the number of droplets, and deformability. It is important to recognize that the droplet confinement is solely a function of flow rate ratio (Q_o/Q_w), whereas deformability mediated by fat crystallization is determined by the coupling between T_{set} and Q_o (as illustrated in Figure 6).

In addition to affecting droplet confinement (and drop deformability indirectly), the carrier fluid flow rate also determines the fluid force needed to push elongated particles through the microcapillary. As a result, we find that the polydispersity of the nonspherical fat particles is significantly higher at low carrier fluid flow rates (see Figure 7a,b). In fact, at the extremely low flow rates (Q_w = 0.5 mL/h) and temperature (T_{set} = 5 °C), we observe that there is not enough fluid force to push the rod-like particles out of the microcapillary, causing them to slow down or completely stop temporarily blocking the fluid flow. This blockage of flow causes significant accumulation of pressure in the system, making the immobilized droplets to exit at very high velocities after the temporary blockage. Because of the repeat of this irregular cycle of slow and extremely fast speed of droplets, droplet production at the orifice is also inconsistent, resulting in very polydisperse particles and irregular frequency of droplet production. Thus, our current setup is amenable to consistent production of only low aspect ratio nonspherical particles (cf. Figure 4e). The maximum aspect ratio of the rod-shaped monodisperse particles obtained in the study was 1.6. The conditions where monodisperse low aspect ratio nonspherical fat particles can be made with a uniform production frequency are highlighted in the dashed region in Figure 4a. To fabricate fat particles of higher aspect ratio, the pressure drop due to the flow of rod-like particles needs to be mitigated. In cylindrical microcapillaries, the presence of a thin symmetric lubrication film between the particle and the tube offers significant resistance for the flow of rod-like particles. However, by modifying the channel cross section to a square, this pressure drop can be reduced because the fluid will now have the opportunity to flow through the angular corners of the square tube.[47]

III.D. Physical Criteria for the Production of Nonspherical Fat Particles. In this section, we discuss the physical basis for the production of nonspherical fat particles using our technique. One obvious physical parameter controlling the asphericity is the ratio of drop size to tube diameter, and it is expected that nonspherical particles are produced when this ratio L_d/D is >1. In addition to this geometric parameter, the competition between the interfacial forces trying to regain the spherical shape of the droplet and the mechanical strength of the fat crystal network trying to resist interfacial deformation is also expected to dictate the ability of fat particles to remain nonspherical. Therefore, for a particle to remain nonspherical, $G' > 2\gamma/R$, where G' is the elastic modulus of the fat crystal network in the droplet and $2\gamma/R$ is the Laplace pressure difference across the interface of the droplet. Here γ is the interfacial tension and R is the radius of curvature. Thus, we expect nonspherical particles to be formed when $L_d/D > 1$ and $G'R/2\gamma > 1$.

To test the applicability of both the geometric ($L_d/D > 1$) and stress ($G'R/2\gamma > 1$) criterion for the production of nonspherical fat particles, we measure L_d for all the different types of particles produced in our experiments. To characterize G', we measure the bulk linear rheology of the palm oil as a function of temperature (cf. Figure 2c) at a cooling rate of 3 °C/min. We assume that the elastic modulus of the fabricated particle is equivalent to the G' value derived from the bulk rheology at the temperature corresponding to T_6 in the microcapillary. The radius of curvature R is estimated to be the radius of the droplets if they are spherical or the radius of the microcapillary when they are nonspherical.

On the basis of the above measurements and estimates, in Figure 8, we plot $G'R/2\gamma$ versus L_d/D. We find as expected nonspherical particles are produced when $L_d/D > 1$. We also found that the nonspherical fat particles lie within the region bounded by $G'R/2\gamma > 1$ and $L_d/D > 1$. Thus, our data seem to

dx.doi.org/10.1021/la401338m | Langmuir 2013, 29, 12307−12316

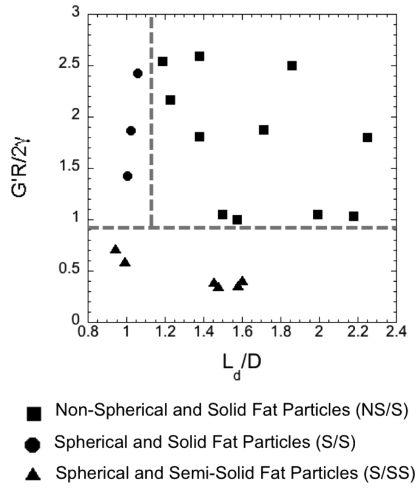

Figure 8. Physical criteria for the production of nonspherical shaped fat particles. The *x*-axis represents the geometric confinement parameter, and the *y*-axis denotes the ratio of elastic modulus to the Laplace pressure. The dashed lines demarcate the regions where different types of fat particles are produced.

be consistent with the geometric and stress criterion for the production of nonspherical particles. However, further validation of the stress criterion is needed because the G' data reported in Figure 2c are derived from bulk rheological experiments conducted at a single cooling rate of 3 °C/min, whereas the conditions under which nonspherical fat particles have been produced correspond to different cooling rates (computed as $(T_1 - T_6)/\tau$, where $\tau = L/U$ is the total residence time) ranging from 1 to 461 °C/min. We attempted to determine the G' values at cooling rates higher than 3 °C/min, but reliable data could not be obtained because of limitations with the rheometer including significant vertical temperature gradient across the gap in the plate−plate geometry, even at marginally higher cooling rates (e.g., 5 °C/min).

Our conceptual model for the production of anisotropic fat particles is similar to models that have been proposed to explain the stability of nonspherical structures formed during arrested coalescence between two Pickering or partially crystalline droplets.[25,26] In these studies, droplets laden with solid particles at the interface or filled internally with wax crystals were forced to coalesce using micromanipulation techniques, and it was found that when the elasticity (due to the Pickering interface or the volume-spanning internal crystal network) dominated the interfacial forces, total coalescence of the drops was prevented, yielding energetically stable nonspherical doublets. Thus, the physical forces for maintaining the nonspherical shape of droplets are similar in this work and prior studies, although in our case confinement of the droplets (in the microcapillary) is a necessary precursor for the production of nonspherical fat particles.

Our results thus far show that drop size and elastic modulus control the nonspherical shape of fat particles. It is also useful to discuss the role of solid fat content in regulating particle shape, as crystallizable fats are typically characterized in terms of SFC. We expect that particles with high SFC will exhibit higher elastic modulus and will therefore better retain the nonspherical shape. In fact, previous studies have shown that the elastic modulus and SFC under quasi-static cooling are related to each other as $G' \sim (\mathrm{SFC})^m$, where m varies between 1.8 and 3.77 for palm oil.[48] Nevertheless, we could not estimate the SFC needed to maintain the nonspherical shape because the SFC data obtained from NMR had significantly different thermal conditions compared to the thermal gradient experienced by the drops in the microfluidic device. In the future, a fat with sharp high melting point (e.g., triglycerides) can be blended with a low melting point liquid oil to quantify the minimum SFC needed to maintain the nonspherical particle shape.

IV. CONCLUSIONS

In this study, we report a new method for the production of spherical and nonspherical fat particles from crystallizable oils. Our results show that there is a strong coupling between fluid flow and external temperature that creates a thermal gradient in the microcapillary. This thermal gradient along with droplet confinement and residence time impacts the degree of crystallinity and shape of the fat particles produced. For the particular case of production of nonspherical particles, the thermal gradient needs to be optimal to allow confined droplets to undergo rapid cooling and develop sufficiently strong elastic fat crystal network to resist the deformation due to interfacial tension. Practically, we find that stage temperature needs to be below the onset temperature of bulk fat crystallization, and carrier fluid flow needs to be high enough to induce rapid cooling as well as provide strong fluid force to transport the confined fat particles.

In this work, we investigated the effect of a single oil flow rate and varied aqueous flow rates. We were able to produce monodisperse dispersions of spherical fat particles of maximum volume fraction of 1 vol %. Nonspherical fat particles were produced with a maximum volume fraction of 4 vol % for monodisperse and 40% for polydiperse emulsions. By pursuing a broader investigation in which both the dispersed and continuous phase flow rates are varied over a wide range may lead to production of monodisperse dispersions of higher volume fraction. Monodisperse rod-like particles of higher aspect ratio can be obtained by modifying the microcapillary to square cross section.

Microfluidic methods provide a high level of control on fluid flow and heat transfer for particle fabrication but are inherently low throughput. The throughput of particle production in this study was 12−36 particles/min. With recent developments in microfabrication and parallelization,[49,50] the particle size could be reduced and throughput increased. For example, tens of microfluidic devices have been assembled in parallel to produce 1 kg/day of double emulsions.[49] Thus, our approach is potentially suited for applications (e.g., pharmaceutics and cosmetics) where products with high value and low volume are acceptable. The benefit that microfluidics provides in this case is control over individual particle properties, 100% yield (since particles are made one by one) and essentially zero loss of active ingredients.

The throughput from microfluidic techniques is not competitive against bulk-scale emulsification methods used in applications such as foods. However, our findings (i.e., identification of regions of different phase behavior and dominant nondimensional parameters) may be translatable to improve bulk emulsification and solidification processes. The well-controlled environment offered by microfluidics enabled us to establish design rules for the production of spherical and nonspherical fat particles, which could have been difficult to glean from bulk-scale processing of crystallizable oils. Given the establishment of design rules, opportunities exist to incorporate

dx.doi.org/10.1021/la401338m | *Langmuir* 2013, 29, 12307−12316

them into conventional processing methods. For example, oil-in-water emulsions made from conventional methods could be forced through thermally cooled membranes that contain cylindrical pores (similar to membrane emulsification[51]), which may allow not only bulk-scale production of spherical and nonspherical fat particles but also of particle sizes much smaller than demonstrated in this study. Thus, our approach and findings could potentially have a significant impact on improving the functionality of products ranging from foods to cosmetics to pharmaceutical creams that incorporate crystallizable fats.

■ ASSOCIATED CONTENT

Supporting Information

Assembly of the cross-junction device; movies of different fat particles exiting from the microcapillary; and gray-scale intensity analysis along the diameter of the fat particles to assess the degree of crystallinity. This material is available free of charge via the Internet at http://pubs.acs.org.

■ AUTHOR INFORMATION

Corresponding Author

*E-mail siva.vanapalli@ttu.edu (S.A.V.).

Notes

The authors declare no competing financial interest.

■ ACKNOWLEDGMENTS

This work was funded by a grant from USDA-AFRI program (Grant No. 2009-02400) and additionally supported by NSF (Grant No. 0967172). We thank Lindsay Wolfe at Penn State University for performing the NMR measurements. We are grateful to Patrick Spicer for useful discussions and sharing their work on anisotropic droplet fabrication prior to publication. John Coupland is acknowledged for providing critical feedback on the manuscript.

■ REFERENCES

(1) Larson, R. G. *The Structure and Rheology of Complex Fluids*; Oxford University Press: New York, 1999.

(2) Hsieh, D. S. T.; Rhine, W. D.; Langer, R. Zero-order controlled-release polymer matrices for micromolecules and macromolecules. *J. Pharm. Sci.* **1983**, *72* (1), 17−22.

(3) Shum, H. C.; Abate, A. R.; Lee, D.; Studart, A. R.; Wang, B. G.; Chen, C. H.; Thiele, J.; Shah, R. K.; Krummel, A.; Weitz, D. A. Droplet microfluidics for fabrication of non-spherical particles. *Macromol. Rapid Commun.* **2010**, *31* (2), 108−118.

(4) Glotzer, S. C.; Solomon, M. J. Anisotropy of building blocks and their assembly into complex structures. *Nat. Mater.* **2007**, *6* (8), 557−562.

(5) Champion, J. A.; Katare, Y. K.; Mitragotri, S. Particle shape: A new design parameter for micro- and nanoscale drug delivery carriers. *J. Controlled Release* **2007**, *121* (1−2), 3−9.

(6) Wang, J.; Byrne, J. D.; Napier, M. E.; DeSimone, J. M. More effective nanomedicines through particle design. *Small* **2011**, *7* (14), 1919−1931.

(7) McClements, D. J. *Food Emulsions: Principles, Practice and Techniques*, 2nd ed.; CRC Press: Boca Raton, FL, 2005.

(8) Hartel, R. W. *Crystallization in Foods*; Springer: Berlin, 2001.

(9) Goff, H.; Hartel, R.W. *Ice Cream*; Springer: Berlin, 2013.

(10) Kabri, T. H.; Arab-Tehrany, E.; Belhaj, N.; Linder, M. Physico-chemical characterization of nano-emulsions in cosmetic matrix enriched on omega-3. *J. Nanobiotechnol.* **2011**. *9*.

(11) Fischer, P.; Eugster, A.; Windhab, E. J.; Schuleit, M. Predictive stress tests to study the influence of processing procedures on long term stability of supersaturated pharmaceutical o/w creams. *Int. J. Pharm.* **2007**, *339* (1−2), 189−196.

(12) Shah, R. K.; Shum, H. C.; Rowat, A. C.; Lee, D.; Agresti, J. J.; Utada, A. S.; Chu, L. Y.; Kim, J. W.; Fernandez-Nieves, A.; Martinez, C. J.; Weitz, D. A. Designer emulsions using microfluidics. *Mater. Today* **2008**, *11* (4), 18−27.

(13) Helgeson, M. E.; Chapin, S. C.; Doyle, P. S. Hydrogel microparticles from lithographic processes: Novel materials for fundamental and applied colloid science. *Curr. Opin. Colloid Interface Sci.* **2011**, *16* (2), 106−117.

(14) Neethirajan, S.; Kobayashi, I.; Nakajima, M.; Wu, D.; Nandagopal, S.; Lin, F. Microfluidics for food, agriculture and biosystems industries. *Lab Chip* **2011**, *11* (9), 1574−1586.

(15) Skurtys, O.; Aguilera, J. M. Applications of microfluidic devices in food engineering. *Food Biophys.* **2008**, *3* (1), 1−15.

(16) Christopher, G. F.; Anna, S. L. Microfluidic methods for generating continuous droplet streams. *J. Phys. D: Appl. Phys.* **2007**, *40* (19), R319−R336.

(17) Seemann, R.; Brinkmann, M.; Pfohl, T.; Herminghaus, S. Droplet based microfluidics. *Rep. Prog. Phys.* **2012**. *75*(1).

(18) Seo, M.; Nie, Z. H.; Xu, S. Q.; Mok, M.; Lewis, P. C.; Graham, R.; Kumacheva, E. Continuous microfluidic reactors for polymer particles. *Langmuir* **2005**, *21* (25), 11614−11622.

(19) Shum, H. C.; Lee, D.; Yoon, I.; Kodger, T.; Weitz, D. A. Double emulsion templated monodisperse phospholipid vesicles. *Langmuir* **2008**, *24* (15), 7651−7653.

(20) Dendukuri, D.; Tsoi, K.; Hatton, T. A.; Doyle, P. S. Controlled synthesis of nonspherical microparticles using microfluidics. *Langmuir* **2005**, *21* (6), 2113−2116.

(21) Fernandez-Nieves, A.; Cristobal, G.; Garces-Chavez, V.; Spalding, G. C.; Dholakia, K.; Weitz, D. A. Optically anisotropic colloids of controllable shape. *Adv. Mater.* **2005**, *17* (6), 680−+.

(22) Xu, S.; Nie, Z.; Seo, M.; Lewis, P.; Kumacheva, E.; Stone, H. A.; Garstecki, P.; Weibel, D. B.; Gitlin, I.; Whitesides, G. M. Generation of monodisperse particles by using microfluidics: Control over size, shape, and composition. *Angew. Chem., Int. Ed.* **2005**, *44* (25), 3799−3799.

(23) Chen, C. H.; Shah, R. K.; Abate, A. R.; Weitz, D. A. Janus particles templated from double emulsion droplets generated using mcrofluidics. *Langmuir* **2009**, *25* (8), 4320−4323.

(24) Wang, B. G.; Shum, H. C.; Weitz, D. A. Fabrication of monodisperse toroidal particles by polymer solidification in microfluidics. *ChemPhysChem* **2009**, *10* (4), 641−645.

(25) Pawar, A. B.; Caggioni, M.; Hartel, R. W.; Spicer, P. T. Arrested coalescence of viscoelastic droplets with internal microstructure. *Faraday Discuss.* **2012**, *158*, 341−350.

(26) Pawar, A. B.; Caggioni, M.; Ergun, R.; Hartel, R. W.; Spicer, P. T. Arrested coalescence in Pickering emulsions. *Soft Matter* **2011**, *7* (17), 7710−7716.

(27) Hu, Y. D.; Wang, Q.; Wang, J. Y.; Zhu, J. T.; Wang, H.; Yang, Y. J. Shape controllable microgel particles prepared by microfluidic combining external ionic crosslinking. *Biomicrofluidics* **2012**, *6* (2), 9.

(28) Zhang, H.; Tumarkin, E.; Sullan, R. M. A.; Walker, G. C.; Kumacheva, E. Exploring microfluidic routes to microgels of biological polymers. *Macromol. Rapid Commun.* **2007**, *28* (5), 527−538.

(29) Liu, K.; Ding, H. J.; Liu, J.; Chen, Y.; Zhao, X. Z. Shape-controlled production of biodegradable calcium alginate gel microparticles using a novel microfluidic device. *Langmuir* **2006**, *22* (22), 9453−9457.

(30) Jiang, K. Q.; Xue, C.; Arya, C. D.; Shao, C. R.; George, E. O.; DeVoe, D. L.; Raghavan, S. R. A new approach to in-situ "micromanufacturing": Microfluidic fabrication of magnetic and fluorescent chains using chitosan microparticles as building blocks. *Small* **2011**, *7* (17), 2470−2476.

(31) Laval, P.; Crombez, A.; Salmon, J. B. Microfluidic droplet method for nucleation kinetics measurements. *Langmuir* **2009**, *25* (3), 1836−1841.

(32) Stan, C. A.; Schneider, G. F.; Shevkoplyas, S. S.; Hashimoto, M.; Ibanescu, M.; Wiley, B. J.; Whitesides, G. M. A microfluidic apparatus

for the study of ice nucleation in supercooled water drops. *Lab Chip* **2009**, *9* (16), 2293−2305.
(33) Toldy, A. I.; Badruddoza, A. Z. M.; Zheng, L.; Hatton, T. A.; Gunawan, R.; Rajagopaan, R.; Khan, S. A. Spherical crystallization of glycine from monodisperse microfluidic emulsions. *Cryst. Growth Des.* **2012**, *12* (8), 3977−3982.
(34) Sgro, A. E.; Allen, P. B.; Chiu, D. T. Thermoelectric manipulation of aqueous droplets in microfluidic devices. *Anal. Chem.* **2007**, *79* (13), 4845−4851.
(35) Ildefonso, M.; Revalor, E.; Punniam, P.; Salmon, J. B.; Candoni, N.; Veesler, S. Nucleation and polymorphism explored via an easy-to-use microfluidic tool. *J. Cryst. Growth* **2012**, *342* (1), 9−12.
(36) Edd, J. F.; Humphry, K. J.; Irimia, D.; Weitz, D. A.; Toner, M. Nucleation and solidification in static arrays of monodisperse drops. *Lab Chip* **2009**, *9* (13), 1859−1865.
(37) Kalustian, P. Pharmaceutical and cosmetic uses of palm and lauric products. *J. Am. Oil Chem. Soc.* **1985**, *62* (2), 431−433.
(38) Stauffer, C. E. The measurement of surface tension by the pendant drop technique. *J. Phys. Chem.* **1965**, *69* (6), 1933−1938.
(39) Tucker, W. B. Surface tension by pendant drops, Massachusetts Institute of Technology, 1938.
(40) Cubaud, T.; Mason, T. G. Capillary threads and viscous droplets in square microchannels. *Phys. Fluids* **2008**, *20* (5), 11.
(41) Fredrick, E.; Walstra, P.; Dewettinck, K. Factors governing partial coalescence in oil-in-water emulsions. *Adv. Colloid Interface Sci.* **2010**, *153* (1−2), 30−42.
(42) Vanapalli, S. A.; Palanuwech, J.; Coupland, J. N. Stability of emulsions to dispersed phase crystallization: effect of oil type, dispersed phase volume fraction, and cooling rate. *Colloids Surf., A* **2002**, *204* (1−3), 227−237.
(43) Garstecki, P.; Stone, H. A.; Whitesides, G. M. Mechanism for flow-rate controlled breakup in confined geometries: A route to monodisperse emulsions. *Phys. Rev. Lett.* **2005**, *94* (16), 4.
(44) Olbricht, W. L. Pore-scale prototypes of multiphase flow in porous media. *Annu. Rev. Fluid Mech.* **1996**, *28*, 187−213.
(45) Vanapalli, S. A.; Banpurkar, A. G.; van den Ende, D.; Duits, M. H. G.; Mugele, F. Hydrodynamic resistance of single confined moving drops in rectangular microchannels. *Lab Chip* **2009**, *9* (7), 982−990.
(46) Cartas-Ayala, M. A.; Raafat, M.; Karnik, R. Self-sorting of deformable particles in an asynchronous logic microfluidic circuit. *Small* **2013**, *9* (3), 375−381.
(47) Wong, H.; Radke, C. J.; Morris, S. The motion of long bubbles in polygonal capillaries. 2. Drag, fluid pressure and fluid-flow. *J. Fluid Mech.* **1995**, *292*, 95−110.
(48) Awad, T. S.; Rogers, M. A.; Marangoni, A. G. Scaling behavior of the elastic modulus in colloidal networks of fat crystals. *J. Phys. Chem. B* **2004**, *108* (1), 171−179.
(49) Romanowsky, M. B.; Abate, A. R.; Rotem, A.; Holtze, C.; Weitz, D. A. High throughput production of single core double emulsions in a parallelized microfluidic device. *Lab Chip* **2012**, *12* (4), 802−807.
(50) Tetradis-Meris, G.; Rossetti, D.; de Torres, C. P.; Cao, R.; Lian, G. P.; Janes, R. Novel parallel integration of microfluidic device network for emulsion formation. *Ind. Eng. Chem. Res.* **2009**, *48* (19), 8881−8889.
(51) Kobayashi, I.; Uemura, K.; Nakajima, M. Generation characteristics of highly uniform nonspherical droplets of soybean oil using microchannel array devices. *Food Biophys.* **2008**, *3* (2), 132−139.